lubricants

MDPI

Article

Significance of Melting Heat Transfer and Brownian Motion on Flow of Powell–Eyring Fluid Conveying Nano-Sized Particles with Improved Energy Systems

Hong Yang [1,2], Aaqib Majeed [3], Kamel Al-Khaled [4], Tasawar Abbas [5], Muhammad Naeem [6], Sami Ullah Khan [6,*] and Munazza Saeed [4]

1 School of Computer Science, Chengdu University, Chengdu 610106, China
2 Key Laboratory of Pattern Recognition and Intelligent Information Processing of Sichuan, Chengdu University, Chengdu 610106, China
3 Department of Mathematics, The University of Faisalabad, Sargodha Road, University Town Faisalabad, Faisalabad 38000, Pakistan
4 Department of Mathematics and Statistics, Jordan University of Science and Technology, P.O. Box 3030, Irbid 22110, Jordan
5 Department of Mathematics, University of Wah, Wah Cantt 47040, Pakistan
6 Department of Mathematics, COMSATS University Islamabad, Sahiwal 57000, Pakistan
* Correspondence: sk_iiu@yahoo.com

Abstract: The present study explores the characteristics of 2D MHD melting with reference to mass and heat transportation upon stagnation point Powell–Eyring nanofluid flow on an extensible surface. Melting is an important phenomenon that is involved in many procedures such as permafrost melting, solidification of slag, defrosting frozen ground etc., all of which are examples of soil freezing and melting that involve heat trafficking through a coil in a grounded pump. A mathematical model is developed for the boundary layer flow. The differential equations are solved through a numerical algorithm which makes use of the boundary value problem solver bvp4c, applying MATLAB software. The numerical variations of embedded parameters on velocity lineation, temperature figuration, and concentration delineation are represented graphically, as are the width of the boundary layer value and the delineation rate for the increasing velocity parameter. The velocity function shows a decremental response for M while the opposite behavior is seen against the concentration field.

Keywords: MHD; melting effects; Powell–Eyring nanofluids; Brownian motion; stagnation point; chemical reaction; mass transfer

Citation: Yang, H.; Majeed, A.; Al-Khaled, K.; Abbas, T.; Naeem, M.; Khan, S.U.; Saeed, M. Significance of Melting Heat Transfer and Brownian Motion on Flow of Powell–Eyring Fluid Conveying Nano-Sized Particles with Improved Energy Systems. *Lubricants* **2023**, *11*, 32. https://doi.org/10.3390/lubricants11010032

Received: 8 December 2022
Revised: 22 December 2022
Accepted: 28 December 2022
Published: 13 January 2023

1. Introduction

Owing to the broad thermal applications of nanoparticles, scientists have specified different applications of such tiny particles in engineering systems, industrial phenomenon and real-world problems. Many challenges related to low-cost energy options can be solved efficiently with modern reforms in nanotechnology, reforms that have given attention to nanoparticles that are considered to have thermal features. In the same way, the versatile significance of this type of metallic nanoparticle also has applications in the medical field, such as destruction of cancer tissues, the diagnosis of various diseases, creation of artificial lungs, and the curing of heart diseases and brain tumors. The improvements to cooling procedures, that enhance different thermal engineering phenomena, mean that solar systems can be upgraded with the use of nanomaterials when compared with base fluids. Nanofluids have recently attracted many researchers to investigate their improved thermal characteristics. Choi [1] proposed the fundamental work on nanofluids. Later, many different investigations were performed on this topic. Buongiorno [2] developed a mathematical model for convective nanofluid flow that included Brownian diffusion and thermophoresis effects. The importance of thermophoresis and Brownian motion effects in nanoparticle/base-fluid slide processes

cannot be overstated. Kuznetsov et al. [3] proposed an analytical solution to the problem of fluid flow under a convective boundary layer across a vertical plate in the presence of nanoparticles. They utilized the influence of thermophoresis and Brownian motion to combine the nanofluid model. Khan and Pop [4] explored effects of nanoparticles on heat transmission and boundary layer flow past a linearly stretching surface. Prasad et al. [5] observed the phenomenon of the heating impact of Williamson nanofluid confined by a rotating disk with mixed convection. Hassan et al. [6] assessed the thermal impact of nanofluids when base fluid viscosity is high. Nadeem et al. [7] investigated a Jeffrey liquid flow model across a stretched surface with nanoparticles. Ramesh et al. [8] expanded on the same experiment but also applied an internal source of heat and magnetic flux. The particle concentration impact on a dusty fluid flow model via porous surface has been explored by Geisha et al. [9]. Ibrahim et al. [10] studied the stagnation point of magneto-hydrodynamic flow with heat transmission of a nanoliquid on a stretchable surface. Madhu and Kishan [11] studied the impact of nanoparticles in a power-law non-Newtonian fluid on an extended sheet with heat source/sink and thermal radiation. Kumari and Gorla [12] presented a theoretical analysis for warm nanoliquid flow to a horizontal melting plate.

In the advanced technology process, melting and solidification phenomena are critical. The melting phenomena of the solid–liquid phase shift have a large scale of applications, including welding, crystal formation, thermal protection, heat transfer, permafrost melting, and semiconductor material preparation. In the beginning, Robert [13] reported the defrosting of ice slabs in heated steam. Hayat et al. [14] investigated the stagnation point flow of Maxwell liquid over a stretchable surface with these melting phenomena. Similarly, the melting process in MHD fluid flow towards a movable surface in heat radiation was explored by Das [15]. Epstein and Cho [16] performed a numerical simulation of melting heat transmission in a stationary panel. Animasaun et al. [17] illustrated mixed convection Newtonian fluid flow towards an upper horizontal thermally stratified melting surface of a paraboloid of revolution. Some related studies are referred in [18–27]. Animasaun et al. [28] explored the impact of the random movement of nanoparticles on various physical dynamic characteristics of fluids. Smith et al. [29] demonstrated how the addition of aluminum oxide nanoparticles augment the viscoelasticity and filtration effects of muds under an HPHT state.

Non-Newtonian nanofluid flow over a stretchable surface has fascinated many scientists due to its wide applications in the field of manufacturing. Its uses in industrial sectors include hot lamination, extruders, manufacturing of fiberglass, melt by fusion, rubber sheets production, the cooling of metallic panels that will be utilized as electrolytes, etc.

Industries produce polymer slips and strings by extruding polymer and winding it up through rollers that stand at a designated distance from one another. The rate of widening of the surface is roughly comparable to the reserve of the hole described by Vleggaar [30]. A detailed description of Powell and Eyring's classical fluid is given in [31]. Therefore, several advantages are concluded for non-Newtonian fluid simulations in the future, including simplicity, the prosperity of calculation and physical strength. The realization of the kinetic theory of fluid, instead of the observed relative, for both share and special rates, contracts Newtonian performance. A stretch tube with adjustable viscosity under certain margin sheet conditions resulted in the flow of Powell–Eyring fluid, as observed by Malik et al. [32]. Powell–Eyring liquid flows, described by Hayat et al. [33], were studied on a shrinking surface under conductive border conditions. There is a Powell–Eyring fluid mentioned in some of the communications of advanced models. In their paper [34], Islam et al. discussed lubricants that disturb Powell–Eyring fluids through homotopy perturbations. Makinde et al. [35] have discussed the dynamics of Casson fluids subject to Lorentz force applied on stratified melting space.

Motivated by these facts, it is noteworthy to explore the volume fraction of nanoparticle impacts on the MHD stagnation point flow of Powell–Eyring liquid with heat and mass transmission. The melting and Brownian effects are considered in the present study. A suitable update is employed to convert the nonlinear PDE's into simple ODE's which are then solved numerically. To demonstrate the effect of pertinent parameters, the result

of concentration, velocity and temperature configurations are drawn pictorially and are represented in tabulated form. To validate the method's accuracy, the present findings show superb accuracy with those previously obtained by [36–40].

The aim of the current research is to present the thermal inspection of heat and mass transfer phenomenon for Powell–Eyring nanofluid subjected to a stagnation point flow. The applications of viscous dissipation and chemical reaction have been endorsed. The analysis is further modified by incorporating the melting heat phenomenon. The motivations for considering the Powell–Eyring fluid model is justified as a limiting case for viscous fluid models that are attained at any shear rate [41–43]. The modelling of this model is based on the theory of kinetic energy of gasses. The numerical computations are based on the shooting technique.

2. Mathematical Modelling

The present analysis focuses on the incompressible stagnation spot of Powell–Eyring nanofluid flow with melting heat transport against a stretched surface at $y = 0$, which can be understood through Figure 1. For the given sheet, we considered x and y axes perpendicular to the surface. This stream is limited to $y \geq 0$. The free stream velocities are assumed as $u_e(x) = ax$ and extendable surface as $u_w(x) = cx$ (a and c indicate positive constants), considering two equal forces in magnitude with opposite direction in such a way that the panel is fixed to the starting point. Hence, the stagnation point flow is calculated. We further considered T_∞ to be larger in value than T_m, which depicts ambient temperature and T_m, which represents melting surface temperature respectively.

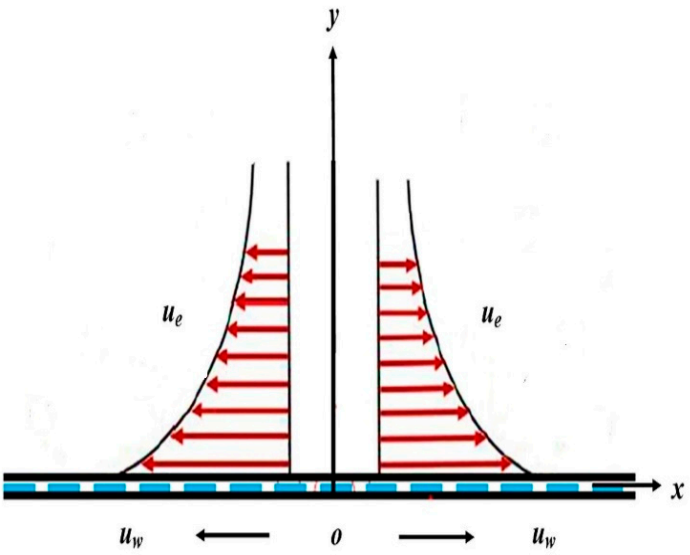

Figure 1. Geometry of the flow problem.

Flow is governed through the following expression [37,39]

$$\frac{\partial u}{\partial x} + \frac{\partial v}{\partial y} = 0, \tag{1}$$

$$\frac{\partial u}{\partial x} + v\frac{\partial u}{\partial y} = \left(1 + \frac{1}{\rho Bc}\right)\frac{\partial^2 u}{\partial y^2} - \frac{1}{2\rho BC^3}\left(\frac{\partial u}{\partial y}\right)^2 \frac{\partial^2 u}{\partial y^2} + u_e\frac{\partial u_e}{\partial x} - \frac{\sigma B_0^2}{\rho}(u - u_e), \tag{2}$$

$$u\frac{\partial T}{\partial x} + v\frac{\partial T}{\partial y} = \alpha\left(\frac{\partial^2 T}{\partial y^2}\right) + \tau\left\{D_B\left(\frac{\partial C}{\partial y}\frac{\partial T}{\partial y}\right) + \frac{D_T}{T_\infty}\left(\frac{\partial T}{\partial y}\right)^2\right\} + 4\mu(1 + \frac{1}{\mu bc})\left(\frac{\partial u}{\partial y}\right)^2 + \frac{\sigma B_0^2 u^2}{\rho C_P}, \tag{3}$$

$$u\frac{\partial C}{\partial x} + v\frac{\partial C}{\partial y} = D_B\frac{\partial^2 C}{\partial y^2} + \frac{D_T}{T_\infty}\frac{\partial^2 T}{\partial y^2} - k\,(c - c_\infty), \tag{4}$$

with boundary conditions:

$$u = u_w = cx, T = T_m, C = C_w,\ k\left(\frac{\partial T}{\partial y}\right)_{y=0} = \rho[\lambda + c_s(T_m - T_0)]v(x,0), \text{at } y = 0, \tag{5}$$

$$u = u_e(x),\ T \to T_\infty,\ C \to C_\infty,\ \text{ as } y \to \infty. \tag{6}$$

where u and v are velocity components along x and y directions, respectively, ρ is fluid density, β is material parameter, T is fluid temperature, k is thermal conductivity, c_p is the specific heat, ν is kinematic viscosity, λ is latent heat, c_s is heat capacity and T_0 is melting surface temperature.

By applying similarity transformation, we have,

$$\eta = y\sqrt{\frac{c}{v}},\ u = cxf'(\eta),\ v = -\sqrt{cv}f(\eta),\ \theta(\eta) = \frac{T - T_\infty}{T_w - T_\infty},\ \varphi(\eta) = \frac{C - C_\infty}{C_w - C_\infty} \tag{7}$$

The following reduction can be achieved when Equation (6) is used to reduce Equations (1)–(4).

$$(1+\epsilon)f''' + ff'' - f'^2 - \in \delta f''^2 f''' + A^2 - Mf' = 0, \tag{8}$$

$$\frac{1}{Pr}\theta'' + f\theta' + Nb\varphi'\theta' + Nt\theta'^2 + (\delta + MEc)f'^2 = 0, \tag{9}$$

$$\varphi'' + Le\, f\varphi' + \frac{Nt}{Nb}\theta'' - K_0\varphi = 0, \tag{10}$$

The corresponding dimensionless boundary conditions are

$$f'(0) = 1, \theta(0) = 0, \varphi(0) = 1,\ Prf(0) + N\theta'(\eta) = 0, \tag{11}$$

$$f'(\infty) = A, \theta(\infty) = 1,\ \varphi(\infty) = 0. \tag{12}$$

where $\epsilon = 1/\mu Bc$ and $\delta = c^3x^2/2\nu c^2$ are Eyring fluid parameters, $A = \frac{a}{c}$ is velocity ratio of a free stream, $N = c_{f(T_\infty - T_m)/\lambda} + c_s\ (T_m - T_o)$ is melting heat transfer parameter, $N_b = \tau(C_w - C_\infty)D_{B/\nu}$ is Brownian motion parameter, $N_t = \tau(T_w - T_\infty)D_B/T_\infty\nu$ is thermophoresis parameter, $M = \frac{\sigma B_0}{\rho c}$ is the Hartmann number, $Le = \frac{\alpha}{D_B}$ is the Lewis number, and $Ec = \frac{u_w^2}{c_p(T_w - T_\infty)}$ is the Eckert number. The dimensionless form of the wall shear force and local Nusselt numbers are [37]:

$$C_f Rex^{\frac{1}{2}} = (1+\varepsilon)f''(0) - \frac{\varepsilon}{3}\delta f''^3(0),\ Nu_x Rex^{-\frac{1}{2}} = -\theta'(0) \tag{13}$$

3. Numerical Scheme

The numerical calculations are achieved by using the shooting technique. The numerical chart of the shooting technique is presented in Figure 2. In simulating the numerical computations, the first order system of the problem is attained by the following assumptions:

$$f = m_1,\ f' = m_2, f'' = m_3, f''' = m'_3, \theta = m_4, \theta' = m_5,\ \theta'' = m'_5$$
$$\varphi = m_6, \varphi\prime = m_7,\ \varphi'' = m\prime_7$$

The dimensionless system (810) in view of the above defined variables becomes:

$$m\prime_3. = -\frac{1}{(1 + \epsilon + \delta\epsilon m_1)}(m_1m_3 + {m_2}^2 - A^2 + Mf') \tag{14}$$

$$m\prime_5 = Pr(-m_1 m_5 - Nbm_6 m_5 - Ntm_5{}^2 - (\delta + MEc)m_2{}^2) \tag{15}$$

$$m\prime_7 = -Le\, m_1 m_6 - \frac{Nt}{Nb} m\prime_5 + K_0 \varphi, \tag{16}$$

The corresponding dimensionless boundary conditions are

$$m_2(0) = 1, m_4(0) = 0, m_6(0) = 1,\ Prm_1(0) + Nm_5(0) = 0, \tag{17}$$

$$m_2(\infty) = A, m_4(\infty) = 1,\ m_6(\infty) = 0. \tag{18}$$

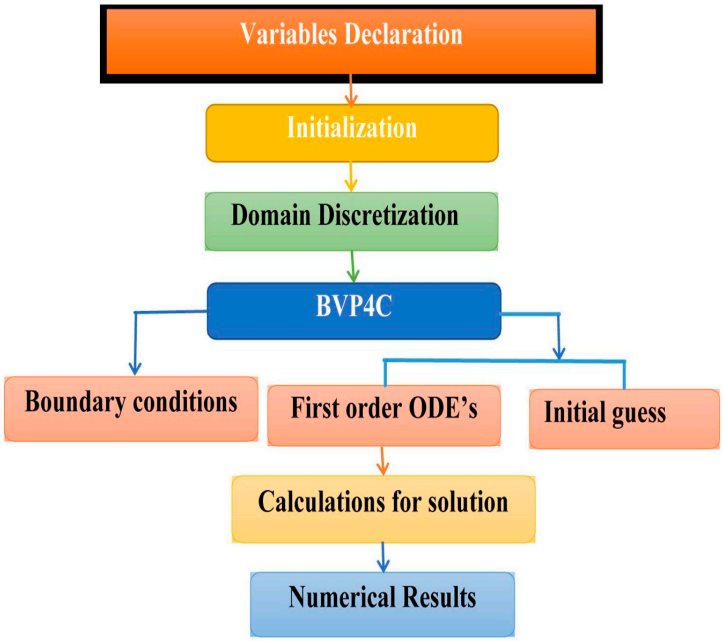

Figure 2. Flow chart of numerical scheme.

4. Validation of Results

The obtained numerical results are verified in Table 1 as a limiting case. The results are compared with the work of Hayat et al. [37] for which analytical computations are performed by using the homotopy analysis method. A fine accuracy between both studies is noted.

Table 1. Comparative analysis for obtained numerical results for $f''(0)$ due with variation of A when $M = \delta = M = N = Ec = 0, Pr = 0.7$.

A	Hayat [37]	Present Results
0.10	−0.96802	−0.968021
0.20	−0.91692	−0.916920
0.50	−0.66722	−0.667222
2.00	2.0175	2.01762
3.00	4.7291	4.72925

5. Results and Discussions

The physical interpretation of parameters governing the flow are observed in this section. The onset of melting parameter N on velocity $f'(\eta)$ is predicted in Figure 3. An enhancing impact in velocity against larger N has been noted. Figure 4 reports the aspect of temperature profile $\theta(\eta)$ for enlarging N. A decreasing variation in temperature profile is exhibited for larger N. Therefore, it is concluded that the melting phenomenon is important to control the thermal phenomenon. Physically, this declining trend is due to fluctuation in temperature in

the melting surface and ambient surface. The observations summarized in Figure 5 reflect the significant of melting parameters N on the concentration profile. For larger melting phenomena, the rate of concentration improved. Figure 6 preserved the observations for $f'(\eta)$ due to Powell–Eyring fluid parameter ε. A rich profile of velocity due to larger ε is noted. Physically, this trend is due to applications of viscoelastic forces. The change in temperature $\theta(\eta)$ due to the enhanced impact of ε is determined in Figure 7. An increasing fluctuation in $\theta(\eta)$ for ε is deduced. However, the declining behavior of $\phi(\eta)$ for ε is evaluated and is reported in Figure 8. The graphical impact of dissipation parameter δ on $\theta(\eta)$ is reflected via Figure 9. The presence of viscous dissipation reflects the strength of the thermal profile. However, the reducing observations for $\phi(\eta)$ are assessed for δ (Figure 10). The impact of the velocity ratio parameter A on $\theta(\eta)$ and $\phi(\eta)$ is examined via Figures 11 and 12, respectively. The enhancing change in $\theta(\eta)$ for large A is claimed. However, contrary observations for $\phi(\eta)$ are depicted for $\phi(\eta)$. The Brownian motion parameter Nb has an impact on temperature $\theta(\eta)$ and concentration $\phi(\eta)$ and is explained in Figures 13 and 14. An enhancing impact of Nb on $\theta(\eta)$ is evaluated. Physically, enhancing change in $\theta(\eta)$ for Nb is due to the Brownian phenomenon. The Brownian phenomenon is based on the random motion of fluid particles due to collision which increases the rate of heat transfer. However, declining aspect of Nb on $\phi(\eta)$ is examined in Figure 14. The lower concentration due to Nb is noted. In fact, a reverse relation of Nb has been noted in the dimensionless concentration equation. Figure 15 shows the onset of the thermophoresis parameter Nt on the concentration profile. An increasing impact of Nt on the concentration profile has been observed. The graphical results summarized in Figure 16 convey the role of Eckert number Ec on $f'(\eta)$. An increment assigning to Ec reports a more enhanced profile of $f'(\eta)$. Physically, such observations are due to applications of the kinetic energy of particles. The effect of Le on $\phi(\eta)$ is displayed in Figure 17. A decline in the concentration profile results when the Lewis number obtains an increasing trend. This decrement in concentration is associated with the low mass diffusivity against an increasing Schmidt number. Figure 18 explains a relation between $\phi(\eta)$ and chemical reaction parameter K_0. It is observed that the concentration profile $\phi(\eta)$ declines for a larger value of K_0. Figures 19 and 20 represent the role of the magnetic parameters M on the concentration profile and velocity field, respectively. A suppression of velocity is noted for larger M. This trend is physically associated with the application of Lorentz forces. However, the concentration profile is enhanced for increasing M.

The wall shear force and Nusselt number variation for numerous values of flow parameters are listed in Table 2. For increasing Pr and ε, an increase in skin friction factor and Nusselt number is noted. However, lower numerical values for these quantities are claimed for A and N.

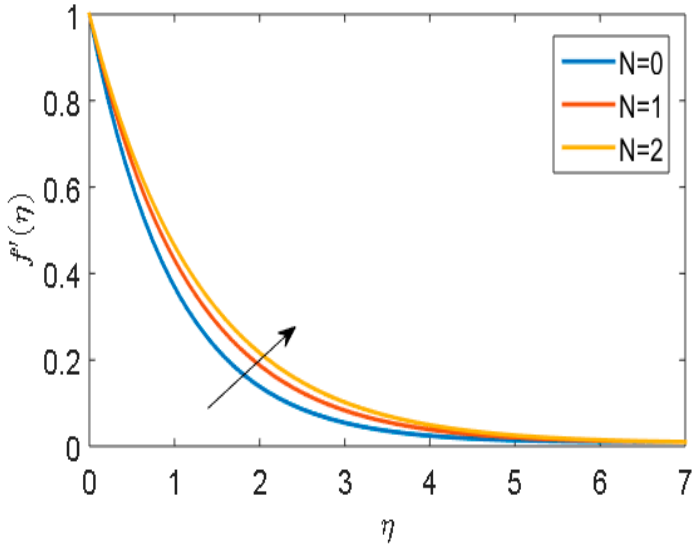

Figure 3. Implication of N on $f'(\eta)$.

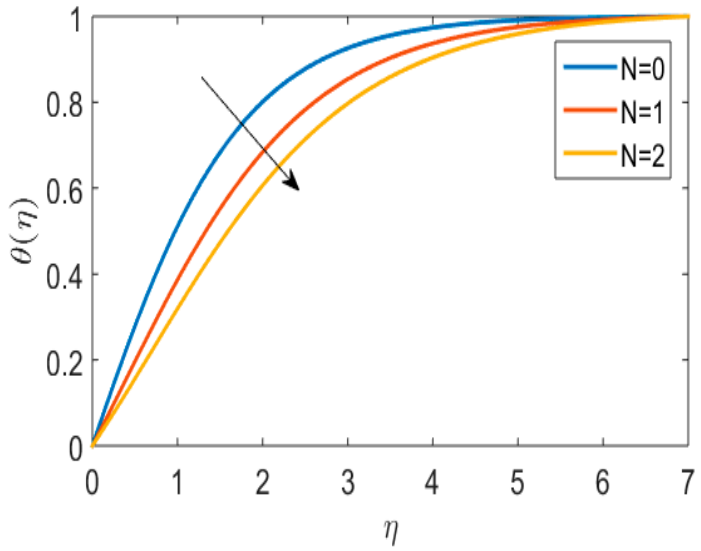

Figure 4. Implication of N on $\theta(\eta)$.

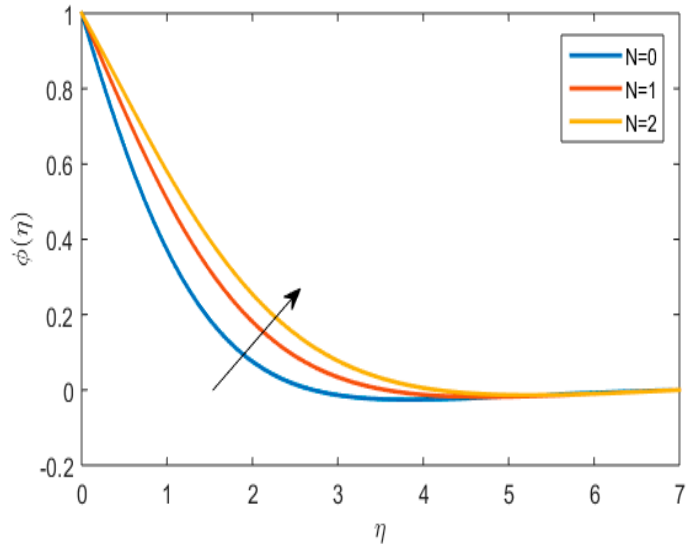

Figure 5. Implication of N on $\phi(\eta)$.

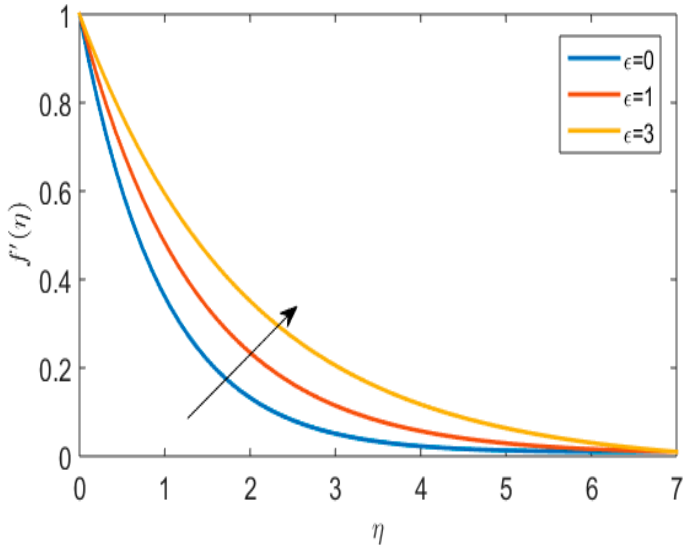

Figure 6. Implication of ε on $f'(\eta)$.

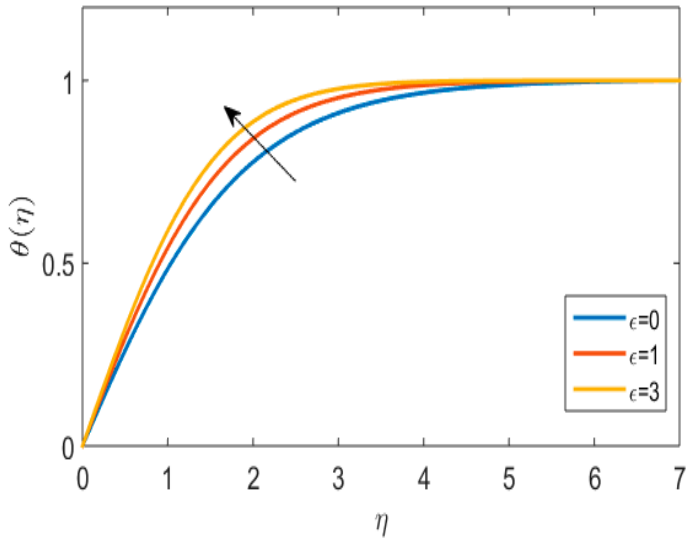

Figure 7. Implication of ϵ on $\theta(\eta)$.

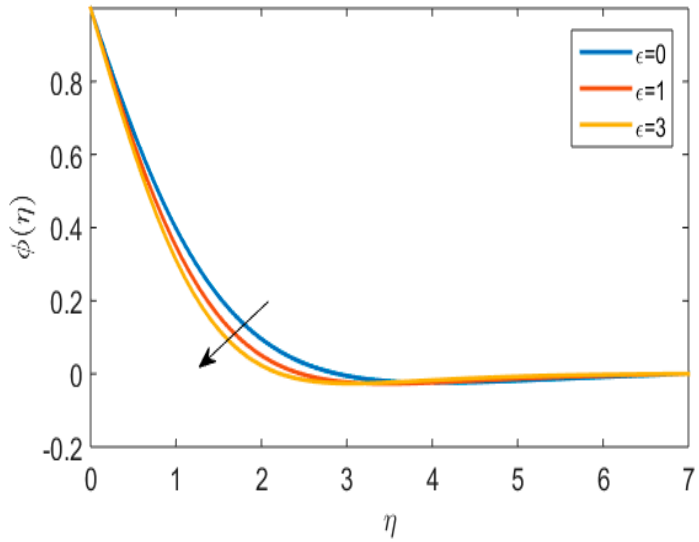

Figure 8. Implication of ϵ on $\phi(\eta)$.

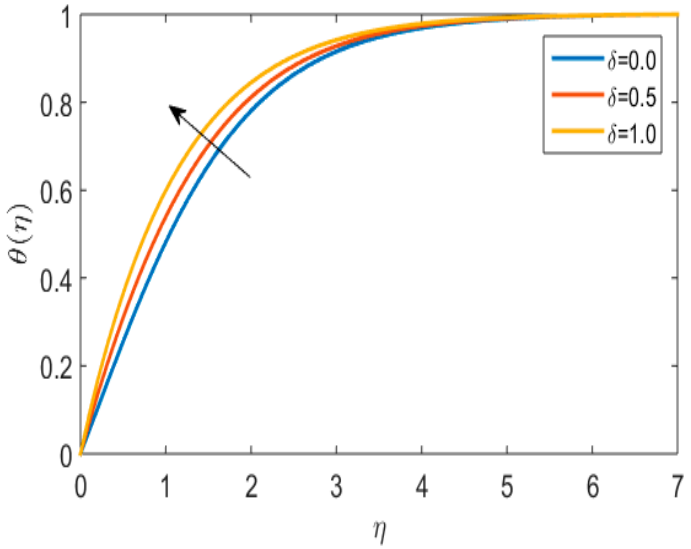

Figure 9. Implication of δ on $\theta(\eta)$.

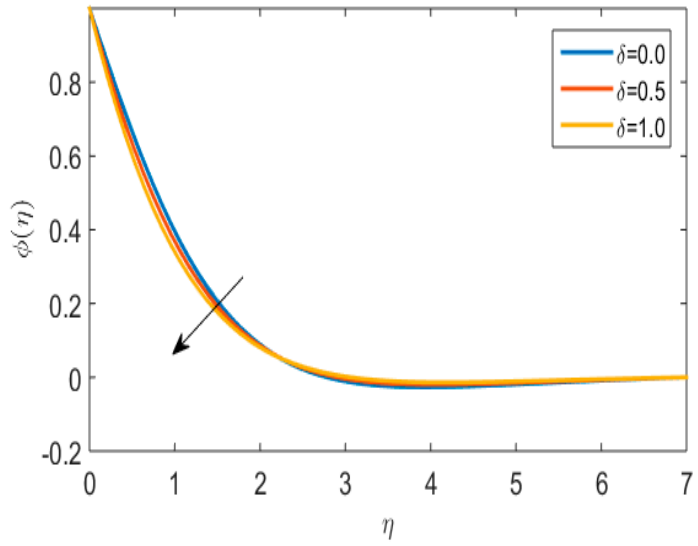

Figure 10. Implication of δ on $\phi(\eta)$.

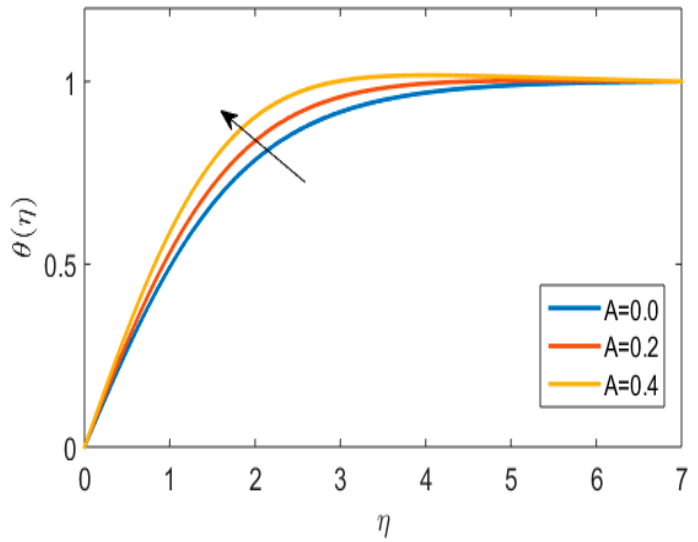

Figure 11. Implication of A on $\theta(\eta)$.

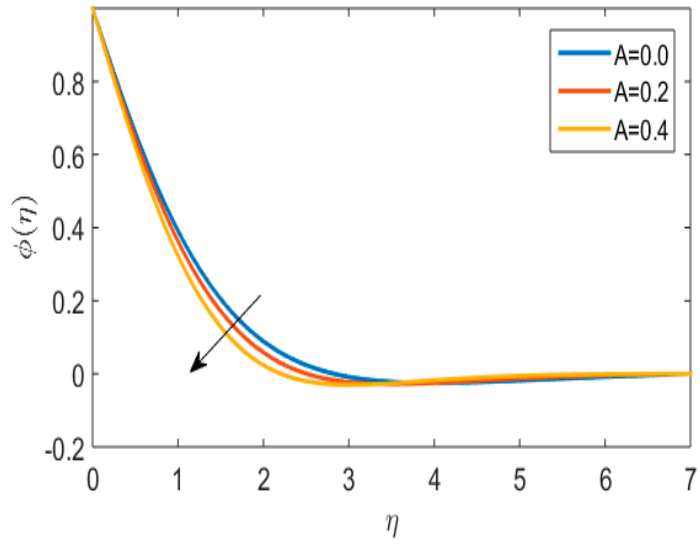

Figure 12. Implication of A on $\phi(\eta)$.

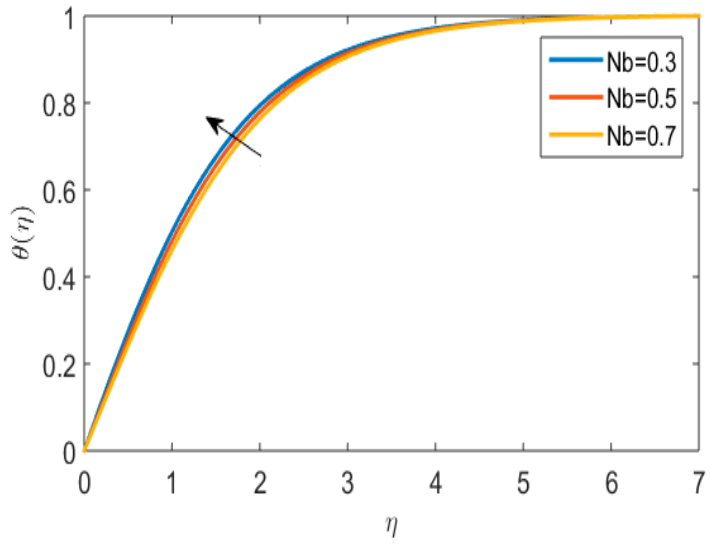

Figure 13. Implication Nb on $\theta(\eta)$.

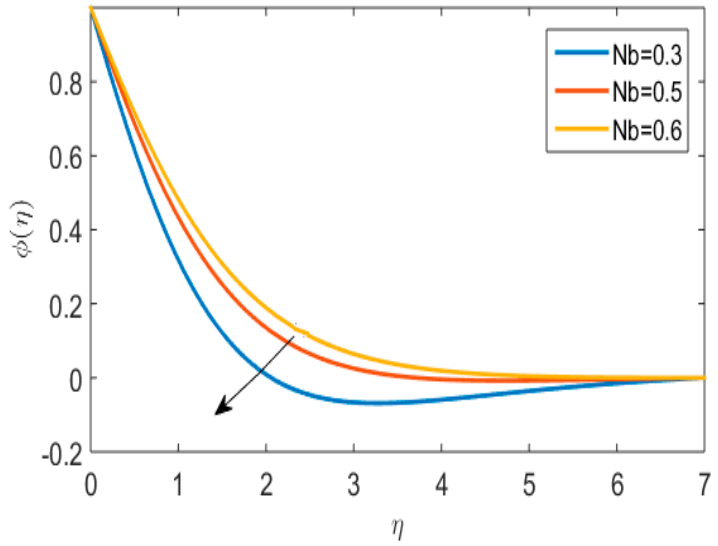

Figure 14. Implication of Nb on $\phi(\eta)$.

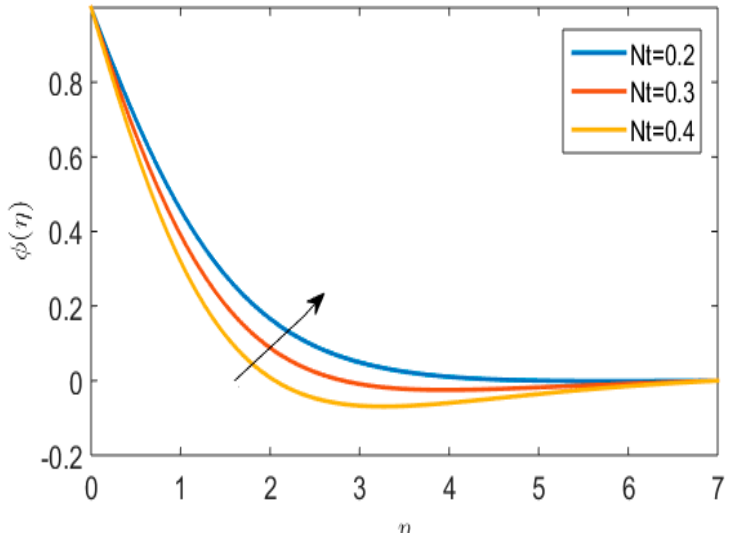

Figure 15. Implication of Nt on $\phi(\eta)$.

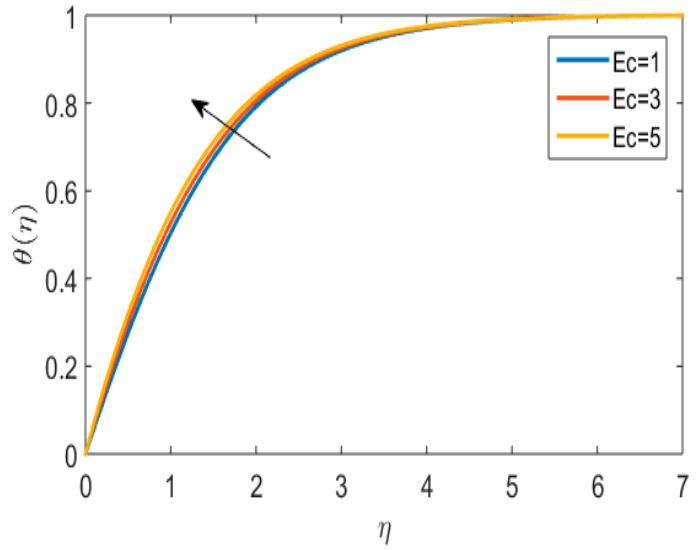

Figure 16. Implication of Ec on $\theta(\eta)$.

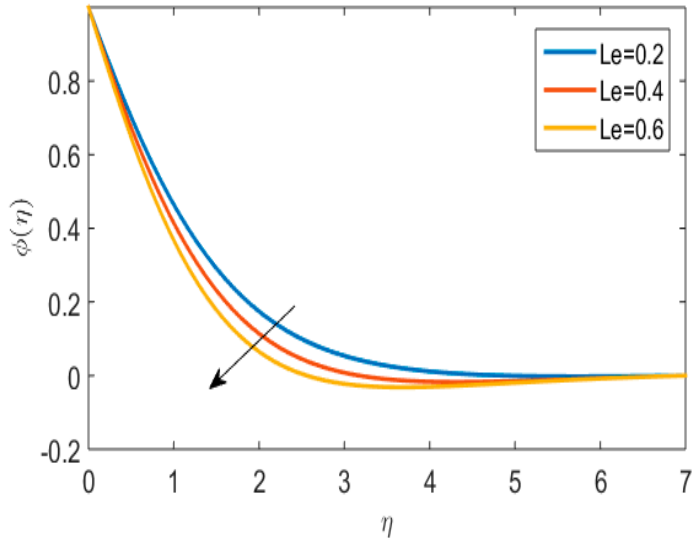

Figure 17. Implication Le on $\phi(\eta)$.

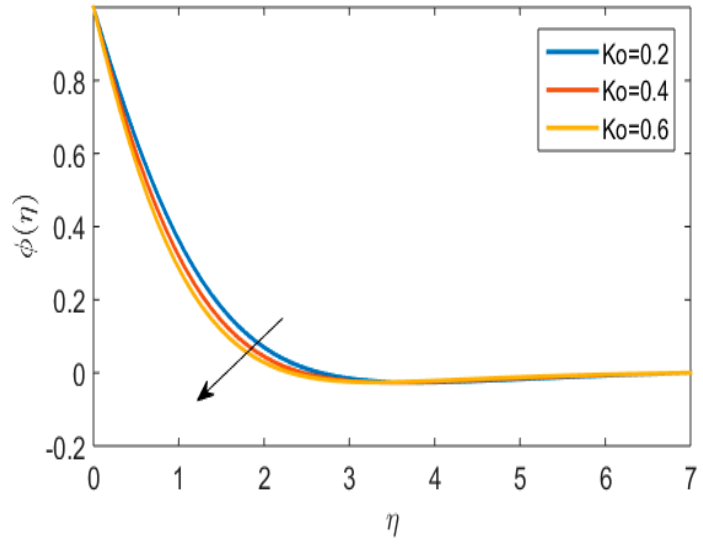

Figure 18. Implication of K_0 on $\phi(\eta)$.

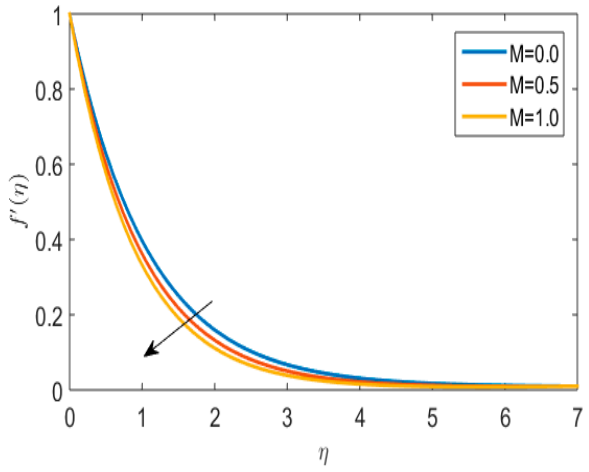

Figure 19. Implication of M on $f'(\eta)$.

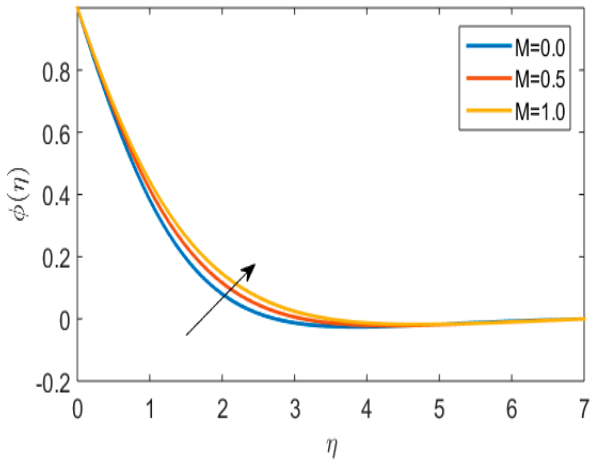

Figure 20. Implication of M on $\theta(\eta)$.

Table 2. Calculation of f'' (0) and $-\theta'$ (0) for N, Pr, ϵ, and A when δ = 0.5.

N	Pr	ϵ	A	$(1+\varepsilon)f''(0)-\frac{\varepsilon}{3}\delta f'^{3}(0)$	$-\theta'(0)$
0.0	1.0	0.5		1.1162	0.7088
0.3				0.7750	0.6910
0.5				0.5490	0.6953
0.8				0.2214	0.7116
	0.8			0.5552	0.7540
	1.0			0.5652	0.8629
	1.2			0.5729	0.9630
		0.0		0.4400	0.8444
		0.5		0.5652	0.8629
		1.0		0.6749	0.8766
		1.2		0.7157	0.8813
			0.0	0.7037	0.7496
			0.2	0.5652	0.8629
			0.5	0.2750	1.0463

6. Conclusions

The thermal impact of Powell–Eyring nanofluid has been studied for stagnation point flow. The application of viscous dissipation and chemical reaction have been considered. The numerical outcomes are presented with the help of the shooting technique. The major outcomes of the analysis are:

- ➢ An enhanced impact in velocity due to the melting heat transfer parameter has been observed.
- ➢ An increase in the thermal profile is observed for melting heat transfer parameter and Powell–Eyring fluid parameter.
- ➢ The temperature profile was enhanced due to Powell–Eyring fluid parameters.
- ➢ With increasing velocity ratio and chemigation reaction constant, the concentration profile declined.
- ➢ For larger Eckert numbers, increasing observations for temperature profile are claimed.

Author Contributions: Conceptualization, H.Y.; methodology, A.M.; software, K.A.-K.; validation, T.A.; formal analysis, M.N.; investigation, S.U.K.; writing—review and editing, M.S. All authors have read and agreed to the published version of the manuscript.

Funding: This work was supported by Sichuan Science and Technology Program under grant 2018ZR0265.

Data Availability Statement: The data used to support the findings of this study are included in the manuscript.

Conflicts of Interest: All the authors declare that they have no conflict of interest.

Nomenclature

(u, v)	velocity components
ρ	fluid density
β	material parameter
T	fluid temperature
k	thermal conductivity
c_p	specific heat
v	kinematic viscosity
λ	latent heat
c_s	heat capacity
T_0	melting surface temperature.
$\in, \delta$	Eyring fluid parameters
A	velocity ratio of a free stream
N	melting heat transfer parameter
N_b	Brownian motion parameter
N_t	thermophoresis parameter
M	Hartmann number
Le	Lewis number
Ec	Eckert number

References

1. Choi, S.U.S. Enhancing thermal conductivity of fluids with nanoparticles. *ASME-Publications-Fed.* **1995**, *231*, 99–106.
2. Buongiorno, J. Convective transport in nanofluids. *J. Heat Transf.* **2006**, *18*, 240–250. [CrossRef]
3. Kuznetsov, A.V.; Nield, D.A. Natural convective boundary-layer flow of a nanofluid past a vertical plate: A revised model. *Int. J. Therm. Sci.* **2014**, *77*, 126–129. [CrossRef]
4. Khan, W.A.; Pop, I. Boundary-layer flow of a nanofluid past a stretching sheet. *Int. J. Heat Mass Transf.* **2010**, *53*, 2477–2483. [CrossRef]
5. Prasad, K.V.; Setty, S.B.; Mebarek-Oudina, F.; Vaidya, H.; Choudhari, R.; Animasaun, I.L. Mixed convective Williamson nanofluid flow over a rotating disk with zero mass flux. *Z. Angew. Math. Mech.* **2022**, *102*, e202100117. [CrossRef]
6. Hassan, M.; Mebarek-Oudina, F.; Faisal, A.; Ghafar, A.; Ismail, A.I. Thermal energy and mass transport of shear thinning fluid under effects of low to high shear rate viscosity. *Int. J. Thermofluids* **2022**, *15*, 100176. [CrossRef]

7. Nadeem, S.; Haq, R.U.; Khan, Z.H. Numerical solution of non-Newtonian nanofluid flow over a stretching sheet. *Appl. Nanosci.* **2014**, *4*, 625–631. [CrossRef]
8. Ramesh, G.K.; Chamkha, A.J.; Gireesha, B.J. Magnetohydrodynamic flow of a non-Newtonian nanofluid over an impermeable surface with heat generation/absorption. *J. Nanofluids* **2014**, *3*, 78–84. [CrossRef]
9. Gireesha, B.J.; Mahanthesh, B.; Gorla, R.S.R. Suspended particle effect on nanofluid boundary layer flow past a stretching surface. *J. Nanofluids* **2014**, *3*, 267–277. [CrossRef]
10. Ibrahim, W.; Shankar, B.; Nandeppanavar, M.M. MHD stagnation point flow and heat transfer due to nanofluid towards a stretching sheet. *Int. J. Heat Mass Transf.* **2013**, *56*, 1–9. [CrossRef]
11. Macha, M.; Kishan, N. Magnetohydrodynamic mixed convection stagnation-point flow of a power-law non-Newtonian nanofluid towards a stretching surface with radiation and heat source/sink. *J. Fluids* **2015**, *2015*, 634186.
12. Mahesh, K.; Gorla, R.S.R. Effect of Melting on Natural Convective Boundary Layer Flow Over a Horizontal Plate Embedded in a Porous Medium Saturated with a Non-Newtonian Nanofluid. *J. Nanofluids* **2014**, *3*, 278–286.
13. Leonard, R. On the melting of a semi-infinite body of ice placed in a hot stream of air. *J. Fluid Mech.* **1958**, *4*, 505–528.
14. Hayat, T.; Farooq, M.; Alsaedi, A.; Iqbal, Z. Melting heat transfer in the stagnation point flow of Powell–Eyring fluid. *J. Thermophys. Heat Transf.* **2013**, *27*, 761–766. [CrossRef]
15. Kalidas, D. Radiation and melting effects on MHD boundary layer flow over a moving surface. *Ain Shams Eng. J.* **2014**, *5*, 1207–1214.
16. Epstein, M.; Cho, D.H. Melting heat transfer in steady laminar flow over a flat plate. *J. Heat Transf.* **1976**, *98*, 531–533. [CrossRef]
17. Animasaun, I.L.; Makinde, O.D.; Saleem, S. Mixed convection flow of Newtonian fluids over an upper horizontal thermally stratified melting surface of a paraboloid of revolution. *J. Braz. Soc. Mech. Sci. Eng.* **2019**, *41*, 1–14. [CrossRef]
18. Gorla, R.R.S.; Mansour, M.A.; Hassanien, I.A.; Bakier, A.Y. Mixed convection effect on melting from a vertical plate in a porous medium. *Transp. Porous Media* **1999**, *36*, 245–254. [CrossRef]
19. Bachock, N.; Ishak, A.; Pop, I. Melting heat transfer in boundary layer stagnation point flow towards a stretching/shrinking sheet. *Phys. Lett.* **2010**, *A374*, 4075–4079. [CrossRef]
20. Anuar, I.; Nazar, R.; Bachok, N.; Pop, I. Melting heat transfer in steady laminar flow over a moving surface. *Heat Mass Transf.* **2010**, *46*, 463–468.
21. Gireesha, B.J.; Mahanthesh, B.; Shivakumara, I.S.; Eshwarappa, K.M. Melting heat transfer in boundary layer stagnation-point flow of nanofluid toward a stretching sheet with induced magnetic field. *Eng. Sci. Technol. Int. J.* **2016**, *19*, 313–321. [CrossRef]
22. Kazmierczak, M.; Poulikakos, D.; Pop, I. Melting from a flat plate embedded in a porous medium in the presence of steady natural convection. *Numer. Heat Transf.* **1986**, *10*, 571–581. [CrossRef]
23. Rahmat, E.; Riaz, A.; Abbasbandy, S.; Hayat, T.; Vafai, K. A study on the mixed convection boundary layer flow and heat transfer over a vertical slender cylinder. *Therm. Sci.* **2014**, *18*, 1247–1258.
24. Riaz, A.; Ellahi, R.; Sait, S.M. Role of hybrid nanoparticles in thermal performance of peristaltic flow of Eyring–Powell fluid model. *J. Therm. Anal. Calorim.* **2021**, *143*, 1021–1035. [CrossRef]
25. Aaqib, M.; Zubair, M.; Khan, A.; Muhammad, T.; Alqarni, M.S. Significance of Thermophoretic and Brownian Motion on MHD Nanofluids Flow towards a Circular Cylinder under the Inspiration of Multiple Slips: An Industrial Application. *Math. Probl. Eng.* **2021**, *2021*, 8634185.
26. Tasawar, A.; Ahmad, B.; Majeed, A.; Muhammad, T.; Ismail, M. Numerical Investigations of Radiative Flow of Viscous Fluid Through Porous Medium. *J. Magn.* **2021**, *26*, 277–284.
27. Majeed, A.; Zeeshan, A.; Xu, H.; Kashif, M.; Masud, U. Heat transfer analysis of magneto-Eyring–Powell fluid over a nonlinear stretching surface with multiple slip effects: Application of Roseland's heat flux. *Can. J. Phys.* **2019**, *97*, 1253–1261. [CrossRef]
28. Animasaun, I.L.; Ibraheem, R.O.; Mahanthesh, B.; Babatunde, H.A. A meta-analysis on the effects of haphazard motion of tiny/nano-sized particles on the dynamics and other physical properties of some fluids. *Chin. J. Phys.* **2019**, *60*, 676–687. [CrossRef]
29. Smith, S.R.; Rafati, R.; Haddad, A.S.; Cooper, A.; Hamidi, H. Application of aluminium oxide nanoparticles to enhance rheological and filtration properties of water based muds at HPHT conditions. *Colloids Surf. A Physicochem. Eng. Asp.* **2018**, *537*, 361–371. [CrossRef]
30. Vleggaar, J. Laminar boundary-layer behaviour on continuous, accelerating surfaces. *Chem. Eng. Sci.* **1977**, *32*, 1517–1525. [CrossRef]
31. Powell, R.E.; Eyring, H. Mechanisms for the relaxation theory of viscosity. *Nature* **1944**, *154*, 427–428. [CrossRef]
32. Malik, M.Y.; Hussain, A.; Nadeem, S. Boundary layer flow of an Eyring–Powell model fluid due to a stretching cylinder with variable viscosity. *Sci. Iran.* **2013**, *20*, 313–321.
33. Hayat, T.; Iqbal, Z.; Qasim, M.; Obaidat, S. Steady flow of an Eyring Powell fluid over a moving surface with convective boundary conditions. *Int. J. Heat Mass Transf.* **2012**, *55*, 1817–1822. [CrossRef]
34. Islam, S.; Shah, A.; Zhou, C.Y.; Ali, I. Homotopy perturbation analysis of slider bearing with Powell–Eyring fluid. *Z. Angew. Math. Phys.* **2009**, *60*, 1178–1193. [CrossRef]
35. Makinde, O.D.; Sandeep, N.; Ajayi, T.M.; Animasaun, I.L. Numerical exploration of heat transfer and Lorentz force effects on the flow of MHD Casson fluid over an upper horizontal surface of a thermally stratified melting surface of a paraboloid of revolution. *Int. J. Nonlinear Sci. Numer. Simul.* **2018**, *19*, 93–106. [CrossRef]

36. Mahapatra, T.R.; Gupta, A.S. Heat transfer in stagnation-point flow towards a stretching sheet. *Heat Mass Transf.* **2002**, *38*, 517–521. [CrossRef]
37. Khan, S.U.; Ali, H.M. Swimming of gyrotactic microorganisms in unsteady flow of Eyring Powell nanofluid with variable thermal features: Some bio-technology applications. *Int. J. Thermophys.* **2020**, *41*, 159. [CrossRef]
38. Song, Y.Q.; Obideyi, B.D.; Shah, N.A.; Animasaun, I.L.; Mahrous, Y.M.; Chung, J. Significance of haphazard motion and thermal migration of alumina and copper nanoparticles across the dynamics of water and ethylene glycol on a convectively heated surface. *Case Stud. Therm. Eng.* **2021**, *26*, 101050. [CrossRef]
39. Jawad, M.; Mebarek-Oudina, F.; Vaidya, H.; Prashar, P. Influence of Bioconvection and Thermal Radiation on MHD Williamson Nano Casson Fluid Flow with the Swimming of Gyrotactic Microorganisms Due to Porous Stretching Sheet. *J. Nanofluids* **2022**, *11*, 500–509. [CrossRef]
40. Sharma, K.; Kumar, S.; Narwal, A.; Mebarek-Oudina, F.; Animasaun, I.L. Convective MHD Fluid flow over Stretchable Rotating Disks with Dufour and Soret Effects. *Int. J. Appl. Comput. Math* **2022**, *8*, 159. [CrossRef]
41. Anjum, N.; Khan, W.A.; Hobiny, A.; Azam, M.; Waqas, M.; Irfan, M. Numerical analysis for thermal performance of modified Eyring Powell nanofluid flow subject to activation energy and bioconvection dynamic. *Case Stud. Therm. Eng.* **2022**, *39*, 102427. [CrossRef]
42. Bhattacharyya, A.; Kumar, R.; Bahadur, S.; Seth, G. Modeling and interpretation of peristaltic transport of Eyring–Powell fluid through uniform/non-uniform channel with Joule heating and wall flexibility. *Chin. J. Phys.* **2022**, *80*, 167–182. [CrossRef]
43. Hussain, M.; Ranjha, Q.A.; Anwar, M.S.; Jahan, S.; Ali, A. Eyring-Powell model flow near a convectively heated porous wedge with chemical reaction effects. *J. Taiwan Inst. Chem. Eng.* **2022**, *139*, 104510. [CrossRef]